Molecular Stacking Induced by Intermolecular C–H···N Hydrogen Bonds Leading to High Carrier Mobility in Vacuum-Deposited Organic Films

Daisuke Yokoyama, Hisahiro Sasabe, Yukio Furukawa, Chihaya Adachi, and Junji Kido*

Simple bottom-up fabrication processes for molecular self-assembly have been developed for the construction of higher-order structures using organic materials, and have contributed to maximization of the potential of organic materials in chemical and bioengineering. However, their application to organic thin-film devices such as organic light-emitting diodes have not been widely considered because simple fabrication of a solid film containing an internal self-assembly structure has been regarded as difficult. Here it is shown that the intermolecular C–H···N hydrogen bonds can be simply formed even in vacuum-deposited organic films having flat interfaces. By designing the molecules containing pyridine rings properly for the intermolecular interaction, one can control the molecular stacking induced by the intermolecular hydrogen bonds. It is also demonstrated that the molecular stacking contributes to the high carrier mobility of the film. These findings provide new guidelines to improve the performance of organic optoelectronic devices and open up the possibilities for further development of organic devices with higher-order structures.

1. Introduction

The intermolecular interaction between organic molecules is one of the most vital characteristics of organic materials when compared with inorganic materials. This interaction makes it possible to construct complicated higher-order structures and to realize multifunctional organic materials. In particular, the variety of the hydrogen bonds[1,2] plays an essential role in controlling the complexity in both chemistry and biology, and has also contributed to maximizing the potential of organic materials in chemical and bioengineering.[3]

However, in the research in organic solid optoelectronic devices, such as organic light-emitting diodes (OLEDs), organic photovoltaic cells (OPVCs), and organic field-effect transistors (OFETs), intermolecular interactions such as hydrogen bonds have not yet been used sufficiently to improve the device performance. This is due to the difficulty in developing a simple bottom-up process for molecular self-assembly to construct higher-order structures in solids. Although molecular self-assembly in a monolayer on a surface has been reported,[4–6] fabrication of a solid film including an internal self-assembly structure of molecules has not yet been demonstrated using a simple process such as vacuum deposition.

In small-molecule OLEDs, for example, vacuum-deposited organic amorphous films have usually been used although they generally have lower carrier mobility than those of polycrystalline films and single crystals. These films are used mainly because they have the advantage of the simple fabrication of multilayer structures with very flat interfaces and high purities without any restrictions on the thicknesses or the underlying layers. However, the intermolecular interactions between the molecules in the films have not been sufficiently investigated since the beginning of research in OLEDs.[7] It has

Dr. D. Yokoyama
Department of Organic Device Engineering
Graduate School of Science and Engineering
Yamagata University
4-3-16 Johnan, Yonezawa, Yamagata 992–8510, Japan
and Center for Future Chemistry
Kyushu University
774 Motooka, Nishi, Fukuoka 819–0395, Japan
E-mail: d_yokoyama@yz.yamagata-u.ac.jp
Dr. H. Sasabe, Prof. J. Kido
Department of Organic Device Engineering
Graduate School of Science and Engineering
Yamagata University
4-3-16 Johnan, Yonezawa, Yamagata 992–8510, Japan
Prof. Y. Furukawa
Department of Chemistry and Biochemistry
School of Advanced Science and Engineering
Waseda University
3-4-1 Okubo, Shinjuku, Tokyo 169–8555, Japan
Prof. C. Adachi
Center for Future Chemistry
Kyushu University
774 Motooka, Nishi, Fukuoka 819–0395, Japan

DOI: 10.1002/adfm.201001919

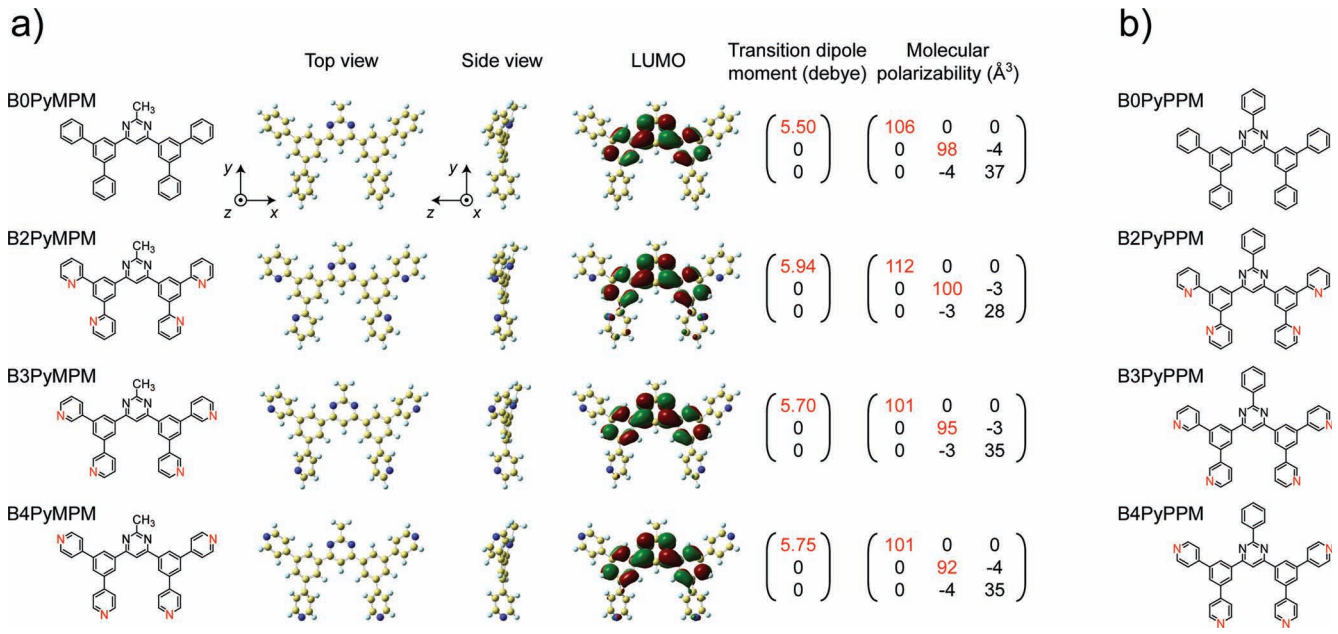

Figure 1. Materials and their properties as a single molecule. a) Chemical structures and properties of B0PyMPM, B2PyMPM, B3PyMPM, and B4PyMPM molecules. For one of the stable conformers of each material, the structure, the LUMO, the largest transition dipole moment in the near-UV region, and the molecular polarizability at 520 nm were determined by DFT calculations. b) Chemical structures of B0PyPPM, B2PyPPM, B3PyPPM, and B4PyPPM molecules.

been taken for granted for around 20 years that the molecular orientation in small-molecule OLEDs is generally random and isotropic. To date, this simple assumption of the random orientation has been available as "the 0th approximation" in the research in OLEDs. At present, however, the device performance of OLEDs has matured to an extent that we must investigate and understand the device physics of OLEDs at the molecular level to further improve their performance and reliability.

Only recently, the intermolecular interaction and the subsequent horizontal molecular orientation in OLEDs have been investigated and reported.[8–12] We have demonstrated the general relationship between the structural anisotropy of a molecule and the molecular orientation in the film.[9,10] The horizontal orientation occurs on any underlying layer[10] and even in isotropic host films,[10,11] and it is almost homogeneous in the direction of the thickness[12] because the effect of the underlying layer does not reach long range into the bulk of amorphous films which do not have a long-range order. The positive effects of the horizontal orientation on the optical[13] and electrical[14,15] properties of the film were also reported, showing the importance of the molecular orientation in vacuum-deposited films for device applications. In addition, the orientation can be controlled from horizontal to vertical by the temperature of a substrate during deposition,[12] which makes the orientation useful for different kinds of organic thin-film devices.

To control the molecular orientation more actively for further improvement of the device performance, it is necessary to use the intermolecular interactions between molecules. Here, we show that the intermolecular C–H···N hydrogen bonds can be formed even in organic vacuum-deposited films having flat interfaces, and demonstrate that the molecular stacking can be controlled by the intermolecular C–H···N hydrogen bonds to improve the carrier mobility of the film. By associating all the data of quantum calculation, ellipsometry, UV–vis spectroscopy, X-ray diffraction (XRD) measurement, IR spectroscopy, and time-of-flight (TOF) measurement, a comprehensive discussion about the effects of the intermolecular hydrogen bonds is presented.

2. Results and Discussion

2.1. Materials

Figure 1 shows the materials used in this study to investigate the intermolecular hydrogen bonds in vacuum-deposited films. We developed four materials, B0PyMPM, B2PyMPM, B3PyMPM, and B4PyMPM, as shown in Figure 1a, to elucidate the effects of the positions of the nitrogen atoms in the pyridine rings, which contribute to the intermolecular C–H···N hydrogen bonds. Also, to confirm the generality, we prepared another series of four similar materials, B0PyPPM, B2PyPPM, B3PyPPM, and B4PyPPM, as shown in Figure 1b, where a phenyl ring is attached instead of a methyl group to the 2-position of the central pyrimidine ring. Some of these materials have been used as electron transport materials in extremely high-performance OLEDs with a power efficiency of more than 100 lm W^{-1}.[16,17] In Figure 1a, we show the structures and the lowest unoccupied molecular orbitals (LUMOs) of a conformer of B0PyMPM and B2–B4PyMPM molecules. From the top and side views of the structures obtained by density functional theory (DFT) B3LYP/6–31G(d) calculations, it was found that the geometric structures of these four materials are almost

the same. The LUMOs also have similar distributions in these molecules, which are mainly located in the central part of the molecules, and not in the terminal phenyl or pyridine rings. The largest transition dipole moments in the near-UV region and the molecular polarizabilities at 520 nm also have similar values and anisotropies, as shown in Figure 1a. The largest transition dipole moments of all four materials obtained by time-dependent DFT B3LYP/6–311+G(d,p) calculations are parallel to the *x*-direction in this figure, and the molecular polarizabilities have much larger diagonal components in the *x*- and *y*-directions than in the *z*-direction.

In Figure 1a, the structure of only one conformer for each molecule was calculated in free space, but there are many other conformers for these materials. This in turn means that the molecules can have many different conformations in vacuum-deposited solid films. However, the LUMOs, transition dipole moments, and molecular polarizabilities of these materials are not heavily dependent on the conformations. This is true not only for B0PyMPM and B2–B4PyMPM, but also for B0PyPPM and B2–B4PyPPM (see Supporting Information Sections 1 and 2 for details).

2.2. Molecular Stacking in Films

In these eight materials, only the vacuum-deposited films of B3PyMPM, B4PyMPM, B3PyPPM, and B4PyPPM have singularly large anisotropies in their optical constants and molecular orientation. **Figure 2**a shows the optical anisotropies of all the films obtained by variable angle spectroscopic ellipsometry

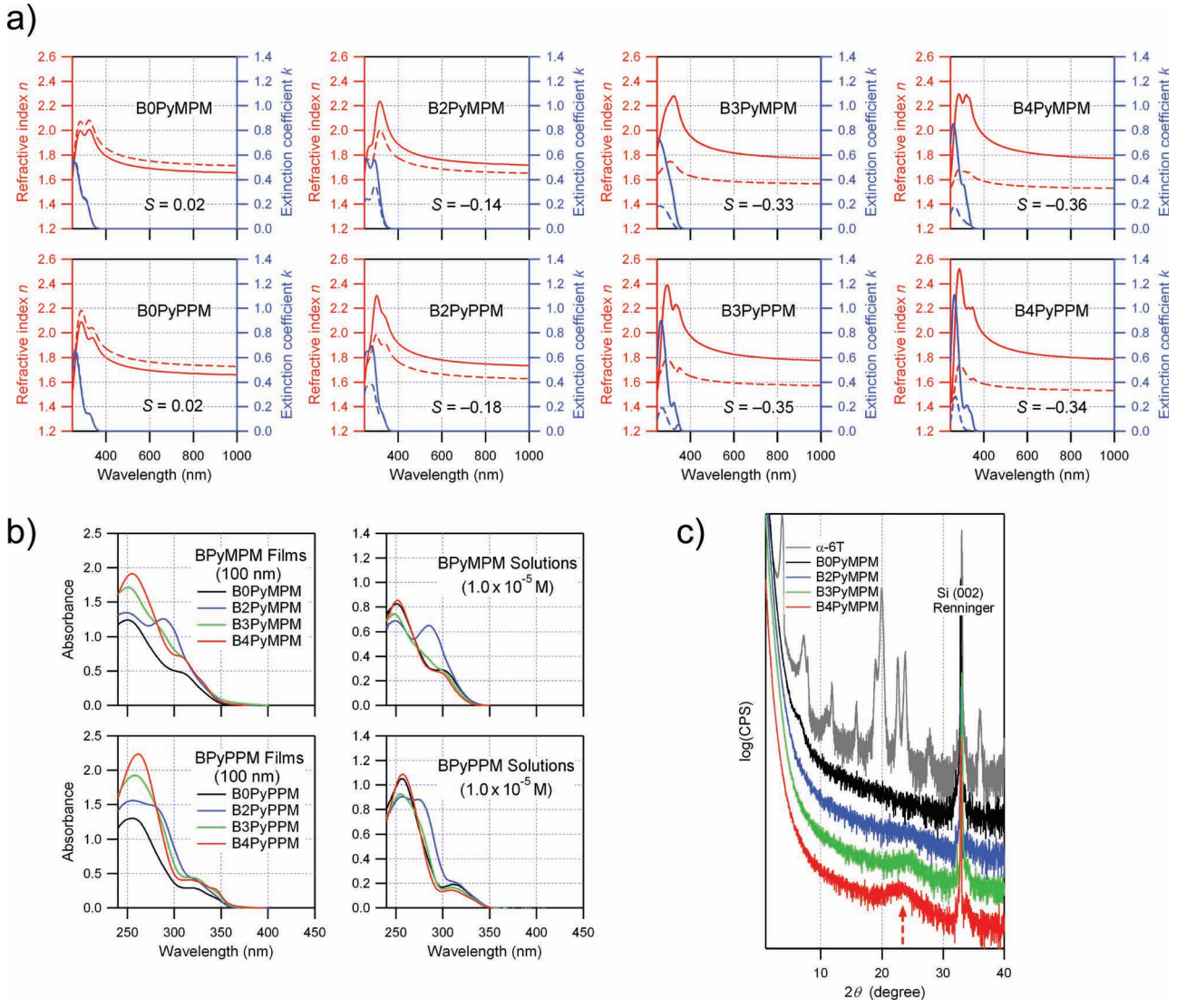

Figure 2. Singularly large anisotropy in B3PyMPM, B4PyMPM, B3PyPPM, and B4PyPPM films by molecular stacking. a) Refractive indices (red) and extinction coefficients (blue) of B0PyMPM, B2–B4PyMPM, B0PyPPM, and B2–B4PyPPM. The solid and broken lines indicate the horizontal and vertical components of the optical constants, respectively. b) Absorption spectra of 100 nm-thick films and solutions with a concentration of 10^{-5} M of B0PyMPM, B2–B4PyMPM, B0PyPPM, and B2–B4PyPPM. c) Out-of-plane XRD patterns of B0PyMPM, B2–B4PyMPM, and α-6T films. The patterns of B3 and B4PyMPM have a halo band, whose peak angle shows the distribution center of the distance of the molecular stacking (red arrow).

(VASE),[9,10,18] where the refractive indices and extinction coefficients are indicated by red and blue colors, respectively, and the solid and broken lines indicate their horizontal and vertical components, respectively. Because the anisotropy in the extinction coefficients of the films shows the anisotropy of the directions of the transition dipole moments in the films, the singularly large differences between the horizontal and vertical components of the extinction coefficients mean that the *x*-directions (see Figure 1a) of the B3PyMPM, B4PyMPM, B3PyPPM, and B4PyPPM molecules are significantly oriented to the horizontal direction in the vacuum-deposited films. The anisotropies in the orientations of the transition dipole moments can be quantified using the orientation order parameter *S*,[9,10,19] whose values for each film are shown in Figure 2a. $S = 0$ if the orientation is completely random, and $S = -0.5$ if the orientation is completely horizontal. The B3PyMPM, B4PyMPM, B3PyPPM, and B4PyPPM films were found to have singularly large absolute values of *S*.

Also, because the anisotropy in the refractive indices of the films shows the anisotropy of the molecular polarizabilities in the films, the singularly large birefringences of the B3PyMPM, B4PyMPM, B3PyPPM, and B4PyPPM films mean that the *x*–*y* planes (see Figure 1a) of these molecules are also significantly oriented to the horizontal direction. Thus, the B3PyMPM, B4PyMPM, B3PyPPM, and B4PyPPM molecules are horizontally oriented in the films, where the molecular planes are nearly parallel to the substrate surface.[9,14]

The difference in the orientation can also be confirmed by comparing the absorbance values of the films. Figure 2b shows the absorbance of 100 nm-thick films and solutions with a concentration of 1.0×10^{-5} M for the eight materials. Here, a chloroform and methanol mixture (99:1 in volume) was used as the solvent of the solutions because B3PyMPM, B4PyMPM, B3PyPPM and B4PyPPM are not sufficiently soluble in chloroform alone. Although the absorbances of the solutions of these materials are similar, the films showed large differences in the absorbance values. These results reflect the differences in molecular orientation between the solutions and the films; the molecular orientations in the solutions are completely random, whereas those in the films depend on the materials. Because the incident light of the spectrometer used in the absorption measurement had its electric field parallel to the substrate surface, the absorbances of the films were affected by the molecular orientation, resulting in the noted difference in the absorbances of the films.[15] For example, the absorbance of the B4PyMPM film was about 1.5 times higher than that of the B0PyMPM film, which corresponds to the theoretical ratio between the complete horizontal and random orientations.

The horizontal orientation with a significantly large anisotropy, such as that seen in the B3PyMPM, B4PyMPM, B3PyPPM, and B4PyPPM films, involves molecular stacking in the films. Figure 2c shows the out-of-plane XRD patterns of the B0PyMPM, B2–B4PyMPM, and α-sexithiophene (α-6T) films, where the α-6T film was used as a reference to show the pattern of a polycrystalline film.[20] The B0PyMPM and B2–B4PyMPM films have no sharp peaks in their XRD patterns. The B3 and B4PyMPM film has a broad halo peak, which shows a periodic structure with a short-range order formed in the direction of the thickness. The 2θ angle at the peak corresponds to the distribution center of the molecular-stacking distance. The estimated distance was ~3.8 Å, which is a reasonable value for the distance between the two planar B3 or B4PyMPM molecules. It should be noted that the halo peak caused by molecular stacking does not mean the formation of a long-range order as seen in polycrystalline films, but only a short-range order as seen in amorphous silicon or an amorphous Alq_3 film.[21] The films of all the materials used have very smooth surfaces, which were quite different from those of polycrystalline films having crystalline molecular grains causing high roughness (see Supporting Information Section 3 for details).

2.3. Permanent Dipole Moments

Because the molecular orientation in the films significantly depends on the positions of the nitrogen atoms in the pyridine rings, we then investigated the reason for this dependence. First, the geometric structures of B2–B4PyMPM are almost the same as those shown in Figure 1a (see also Supporting Information Section 1 for details). Thus, the differences in the molecular orientations are not caused by the structural anisotropy of the molecules, showing that the mechanism of the orientation for B3 and B4PyMPM differs from that reported previously.[9,10]

Next, we considered the effect of the permanent dipole moments on the orientation, because the electrostatic energy of a large dipole-dipole interaction can cause alignment of the molecular orientations. To compare the permanent dipoles of the B2–B4PyMPM, the effect of the directions of the pyridine and pyrimidine rings should be taken into account, as shown in **Figure 3**a. Each pyridine and pyrimidine ring in these molecules has a local permanent dipole moment of 2.2–2.3 debye (see Supporting Information Section 4 for details), whose directions are shown by the blue arrows. The permanent dipole moment of a single molecule is mainly determined by the sum of these vectors. However, in the case of the B2 and B3PyMPM, it depends on the dihedral angles between a pyridine ring and the neighbor phenyl ring because the rotations of the pyridine rings, which are schematically shown by the light blue arrows, change the direction of the local permanent dipole moments of the pyridine rings, whereas the permanent dipole moment of the B4PyMPM molecule does not depend on the rotation of the pyridine rings. Thus, to discuss the permanent dipole moments of the molecules, we have to consider the effect of the conformation on them. To extract the qualitative differences between the molecules, we calculated the permanent dipole moments of the B2–B4PyMPM molecules having two kinds of geometric structure, as shown in Figure 3b. For each structure, the B2 and B3PyMPM molecules have 16 ($=2^4$) conformers due to the differences in the directions of the nitrogen atoms in the pyridine rings (see also Supporting Information Section 1 for details), whereas the B4PyMPM molecule has only one conformer for each structure. For all of these conformers, the molecular structures were optimized by B3LYP/6–31G(d) calculations, and the permanent dipole moments were also obtained. As shown in Figure 3b, those of the B2 and B3PyMPM molecules significantly depend on the conformations. The B4PyMPM molecule has one value for each structure, and the values in total are much less than those of the B2 and B3PyMPM molecules. This

is because the vectors of the local permanent dipole moments of the pyridine and pyrimidine rings in the B4PyMPM molecule have different directions and cancel each other out. Therefore, the permanent dipole moment is not a main factor in the control of the molecular orientation in the films.

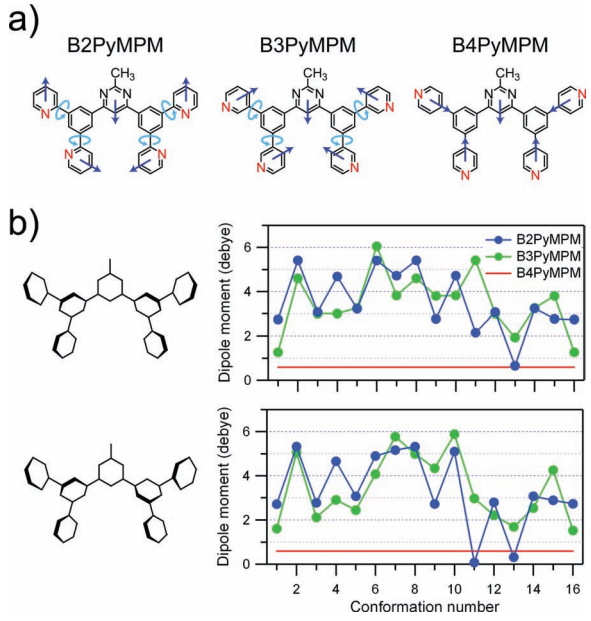

Figure 3. Permanent dipole moments. a) Directions of the local permanent dipole moments of pyridine and pyrimidine rings in B2–B4PyMPM. The sum of the vectors contributes greatly to the permanent dipole moment of a molecule. b) Permanent dipole moments of single molecules of B2–B4PyMPM with two types of geometric structures. For B2 and B3PyMPM, both the geometric structures have 16 conformers due to the difference in the directions of the four pyridine rings, whereas those of B4PyMPM have only one conformer. All of the dipole moments were obtained using the structures optimized by B3LYP/6–31G(d) calculations.

2.4. Intermolecular C–H···N Hydrogen Bonds

The singularly larger anisotropies in the B3 and B4PyMPM films when compared with that in the B2PyMPM film can be explained only by the intermolecular C–H···N hydrogen bonds between the molecules. Because the B3 and B4PyMPM molecules have the nitrogen atoms in the pyridine rings at the outer side of the molecule, they can be connected by the intermolecular C–H···N hydrogen bonds (see Supporting Information Section 4 for details). The high solubility of B3 and B4PyMPM in chloroform with a small amount of methanol also indicates that the intermolecular hydrogen bonds are broken by methanol. Examples of the interactions between the B3PyMPM molecules and between the B4PyMPM molecules are shown in **Figure 4**a and 4b, respectively. Using molecules having a quite similar chemical structure, it was reported that the intermolecular C–H···N hydrogen bonds and the subsequent two-dimensional networks were directly observed at the interface between a solution and a graphite surface by scanning tunnelling microscopy (STM) measurements.[22–26] Therefore, we can suppose that the hydrogen bonds would be formed even in the vacuum-deposited films (see Supporting Information Section 5 for details).

To demonstrate direct evidence of the formation of the intermolecular C–H···N hydrogen bonds in the vacuum-deposited films, we measured the IR absorption spectra of the B2–B4PyMPM films. It has been reported that the formation of weak hydrogen bonds such as C–H···N and C–H···O interactions causes a blue shift in the frequency of the C–H stretching mode.[27–32] Because it is impossible to prepare solutions of B2–B4PyMPM

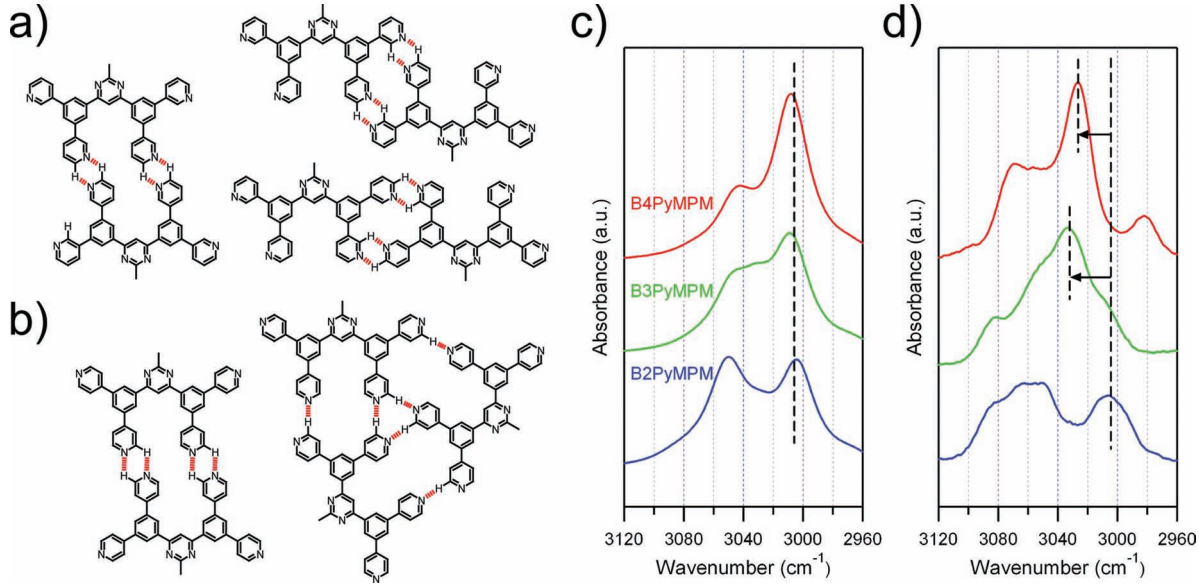

Figure 4. Intermolecular C–H···N hydrogen bonds in films. a,b) Examples of interactions between B3PyMPM molecules (a) and between B4PyMPM molecules (b) by intermolecular C–H···N hydrogen bonds. c) IR absorption spectra of single molecules of B2–B4PyMPM simulated by B3LYP/6–31G(d,p) calculations. The main peaks of all three molecules at lower frequency have almost the same peak frequency as indicated by the broken line. d) IR absorption spectra of the vacuum-deposited films of B2–B4PyMPM. The main bands of B3 and B4PyMPM were blue-shifted compared with that of B2PyMPM.

using a nonpolar solvent to observe the IR spectra of the isolated molecules, we simulated the IR spectra of the B2–B4PyMPM single molecules in free space, as shown in Figure 4c, where the optimized structures and frequencies were obtained by B3LYP/6–31G(d,p) calculations. To compare them with the observed spectra of the films shown in Figure 4d, we assumed a bandwidth of 15 cm^{-1} for all the vibrational modes and a scaling factor[33] of 0.95. The spectral region around 3000 cm^{-1} was focused on because the frequencies of the C–H stretching modes, which are affected by the intermolecular C–H···N hydrogen bonds, are in this region. As shown in Figure 4c, the main peaks in all the simulated spectra have similar frequencies of ~3000 cm^{-1}. These main peaks are attributed to the C–H vibrational modes at the neighbors of the nitrogen atoms in the pyridine rings (see Supporting Information Section 6 for details). Thus, the formation of the intermolecular hydrogen bonds as shown in Figure 4a and 4b causes the blue shift of the main peaks in the actual spectra of the B3 and B4PyMPM films. In the measured spectra of the B3 and B4PyMPM films in Figure 4d, the main peaks are actually blue-shifted as compared with that of the B2PyMPM film, showing that the intermolecular C–H···N hydrogen bonds are formed between the molecules in the B3 and B4PyMPM films.

2.5. Effects on Electron Transport Characteristics

We then investigated the difference in the TOF electron mobilities of the B2–B4PyMPM films to clarify the effect of the orientation on the electrical characteristics of the devices. **Figure 5**a shows the dependence of the electron mobilities on the electric field at 298 K.[34] The B3PyMPM film has a one-order higher mobility than the B2PyMPM film, and the B4PyMPM film has a further one-order higher mobility. To examine the difference further, we also measured the dependence of the mobilities on temperature and electric field and analyzed the results using Bässler's formalism,[35] where the dependences are interpreted using the energetic and positional disorders, σ and Σ. The results of the measurement were reported in our previous paper,[34] and the mobilities and the disorders are summarized in **Table 1**. By associating these results with all the data in this study, we can comprehensively discuss the effect of the molecular stacking on the electrical characteristics of the films as below.

Table 1. TOF electron mobilities and disorder parameters of B2–4PyMPM films.[34] The electron mobilities μ_e were determined by the TOF measurements at 298 K and an electric field of 6.4×10^5 V cm^{-1}. The energetic and positional disorders, σ and Σ, were estimated using the dependences of the TOF mobilities on temperature and electric field.

	μ_e[cm^2 $V^{-1}s^{-1}$]	σ[meV]	Σ
B2PyMPM	1.6×10^{-6}	91	2.7
B3PyMPM	1.5×10^{-5}	88	1.2
B4PyMPM	1.0×10^{-4}	76	0.6

Generally, the energetic disorder in the films becomes larger as the local field caused by the permanent dipole moment of the molecules increases, and the positional disorder becomes larger as the packing constraints between the molecules weaken.[36] Because the B4PyMPM molecules have smaller permanent dipole moments than those of the B2 and B3PyMPM molecules, the energetic disorder in the B4PyMPM film is less than those in the B2 and B3PyMPM films. Then, because the B3 and B4PyMPM molecules are well horizontally oriented in the films, the positional disorders in these films are less than that in the B2PyMPM film. These differences in the disorders affect the electron mobilities of the films as schematically shown in Figure 5b. We emphasize that the intermolecular hydrogen bonds do not directly contribute to the improvement of the electrical properties, but the subsequent molecular stacking induced by them contributes significantly. This result shows the significant effects of both the molecular orientation and the permanent dipole moment on the electrical characteristics of the organic devices. It is also shown that we can control the molecular stacking via the intermolecular hydrogen bonds even in vacuum-deposited organic films to improve the performance of organic thin-film optoelectronic devices such as OLEDs.

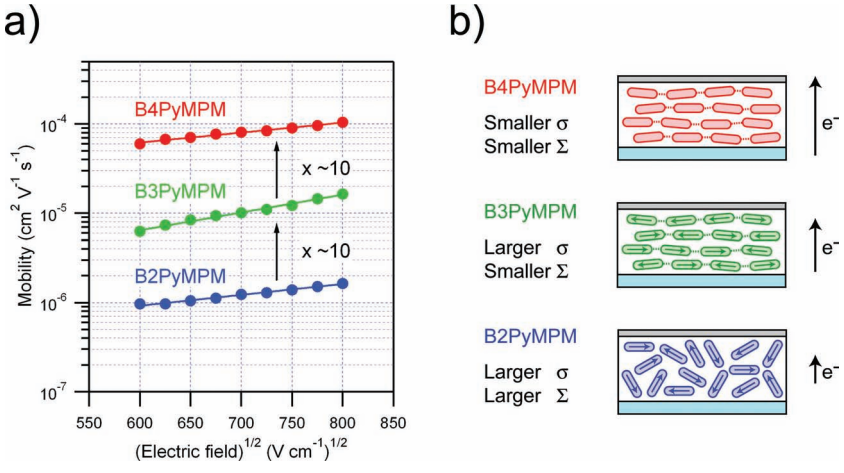

Figure 5. Effects on electron mobility. a) Dependences of electron mobilities of B2–B4PyMPM films on electric field obtained by TOF measurements at 298 K.[34] b) Schematic illustration of the effects of the molecular orientation and the permanent dipole moment on the electrical properties of the B2–B4PyMPM devices. The B3 and B4PyMPM molecules are bound by the intermolecular hydrogen bonds and form the stacking structure in the films. The arrows in the molecules indicate the large permanent dipole moments of the molecules.

Further possibilities exist for use of the molecular orientation to investigate organic device physics and to improve device performance. We can expect that the molecular orientation as seen in the B3 and B4PyMPM films can further contribute to the improvement of the properties of the interface between an organic layer and an electrode, because the interaction between the molecules and the electrode is of vital importance for charge injection.[37] This can improve the performance not only of OLEDs but also of OPVCs and OFETs. In addition, the horizontal molecular orientation also

significantly affects the optical properties of films. For example, the horizontal orientation makes the refractive index for horizontally polarized light very high.[9] Because horizontally polarized light is the main contributor to the outcoupling of OLEDs,[38] a large birefringence in the charge transport layer requires modification of the outcoupling simulation. A high refractive index is preferable for electron transport materials to optimize the interference effect in OLEDs using a thin layer, leading to the compensation of their low electron mobility.

3. Conclusions

To investigate the intermolecular interaction of pyridine-containing electron transport materials used in OLEDs, we analyzed the molecular orientation and stacking in vacuum-deposited films of B0PyMPM, B2–B4PyMPM, B0PyPPM, and B2–B4PyPPM by ellipsometry, UV–vis absorption measurement, XRD measurement, and quantum calculation. The results show that the molecular planes of the B3PyMPM, B4PyMPM, B3PyPPM, and B4PyPPM molecules are singularly oriented parallel to the substrate surface. The singular orientation is caused not by the structural anisotropy or the permanent dipole moments of the molecules, but by the intermolecular C–H···N hydrogen bonds between the molecules in the films. Because the B3PyMPM, B4PyMPM, B3PyPPM, and B4PyPPM molecules have the nitrogen atoms in the pyridine rings at the outer side of the molecule, they can be connected by the intermolecular C–H···N hydrogen bonds, resulting in the blue-shift of the IR absorption frequency of the C–H stretching mode.

We also demonstrate that the molecular stacking induced by the intermolecular hydrogen bonds contributes to the high carrier mobility in the film. By associating all the data in this study with the results of the TOF measurement that we previously reported, we showed that both the molecular orientation and the permanent dipole moment significantly affect the electrical characteristics of the organic devices.

These findings provide much insight to develop new materials for the improvement of the performance of organic thin-film optoelectronic devices such as OLEDs. By designing the molecules properly for the intermolecular hydrogen bonds, we can control the molecular stacking via the intermolecular hydrogen bonds even in vacuum-deposited organic films to improve device characteristics.

The control of the molecular orientation in vacuum-deposited films by the intermolecular hydrogen bonds also opens up the new possibility that we can fabricate multilayer thin-film structures with designed orientation and thicknesses in each layer freely, irrespective of the underlying layer. Finally, by controlling the molecular orientation with a higher order, a simple bottom-up fabrication process for three-dimensional molecular networks can be expected in the future.

4. Experimental Section

Synthesis and Characterization of the Materials: See Supporting Information Section 7.

Fabrication of Sample Films: All of the organic layers were deposited in a vacuum of $<3 \times 10^{-3}$ Pa at an evaporation rate of ~0.2 nm s^{-1}. Films with a thickness of 100 nm were deposited on cleaned substrates. Bare silicon (100) substrates were used for ellipsometry, XRD measurement, and atomic force microscopy (AFM). Fused silica substrates were used for the measurement of the UV-vis absorption spectra. BaF_2 substrates were used for measurement of the IR spectra.

Ellipsometry Measurements: Variable angle spectroscopic ellipsometry (VASE) measurements for the films on Si substrates were performed using a fast spectroscopic ellipsometer (M-2000U, J. A. Woollam Co., Inc.) at seven angles of incident light from 45° to 75° in steps of 5°. At each angle, the experimental ellipsometric parameters Ψ and Δ were simultaneously obtained in steps of 1.6 nm throughout the spectral region from 245 nm to 1000 nm. The analysis of all the combined VASE data was performed using the "WVASE32" software (J. A. Woollam Co., Inc). The method used to determine the anisotropic optical constants is described in detail in refs.[9,10]

Measurement of Absorption Spectra, XRD patterns, AFM images, and IR Spectra: UV–vis absorption spectra of the films and solutions were measured using a UV–vis-NIR spectrophotometer (Shimadzu Co., UV-3150). XRD measurements were performed using a high-resolution XRD diffractometer (SmartLab, Rigaku Co.). Cu K_α radiation was used at 45 kV and 200 mA. The width of the divergence, scattering, and receiving slits were 1, 1, and 1 mm, respectively. The 2θ values were scanned from 3° to 40° in steps of 0.01° with scanning speeds of 5° min^{-1}. AFM images were obtained using a scanning probe microscope (JSPM-5400, JEOL Ltd.). IR spectra were measured using an FTIR spectrometer (FTS7000e, Varian Inc.).

Supporting Information

Supporting Information is available from the Wiley Online Library or from the author.

Acknowledgements

We acknowledge the Rigaku Corporation for helping us measure the XRD patterns of the films. We thank Mr. M. Miyamura (Waseda University) for helping us measure the IR absorption spectra. We also thank the Research Center for Computational Science (RCCS), Okazaki National Research Institutes for the use of a SGI Altix4700 computer. This work was supported by the Promotion of Environmental Improvement for Independence of Young Researchers Program of the Ministry of Education, Culture, Sports, Science and Technology, Japan. This work was also partly supported by the Konica Minolta Imaging Science Foundation.

Received: September 13, 2010
Revised: December 10, 2010
Published online: March 11, 2011

[1] G. A. Jeffrey, in *An Introduction to Hydrogen Bonding* , Oxford Univ. Press, New York **1997**.
[2] G. R. Desiraju, T. Steiner, in *The Weak Hydrogen Bond: In Structural Chemistry and Biology*, Oxford Univ. Press, New York, US **1999**.
[3] E. A. Meyer, R. K. Castellano, F. Diederich, *Angew. Chem. Int. Ed.* **2003**, *42*, 1210.
[4] L. Bartels, *Nat. Chem.* **2010**, *2*, 87.
[5] T. Yokoyama, S. Yokoyama, T. Kamikado, Y. Okuno, S. Mashiko, *Nature* **2001**, *413*, 619.
[6] G. Pawin, K. L. Wong, K.-Y. Kwon, L. Bartels, *Science* **2006**, *313*, 961.
[7] C. W. Tang, S. A. VanSlyke, *Appl. Phys. Lett.* **1987**, *51*, 913.
[8] H.-W. Lin, C.-L. Lin, H.-H. Chang, Y.-T. Lin, C.-C. Wu, Y.-M. Chen, R.-T. Chen, Y.-Y. Chien, K.-T. Wong, *J. Appl. Phys.* **2004**, *95*, 881.
[9] D. Yokoyama, A. Sakaguchi, M. Suzuki, C. Adachi, *Appl. Phys. Lett.* **2008**, *93*, 173302.

[10] D. Yokoyama, A. Sakaguchi, M. Suzuki, C. Adachi, *Org. Electron.* **2009**, *10*, 127.
[11] J. Frischeisen, D. Yokoyama, C. Adachi, W. Brütting, *Appl. Phys. Lett.* **2010**, *96*, 073302.
[12] D. Yokoyama, C. Adachi, *J. Appl. Phys.* **2010**, *107*, 123512.
[13] H.-W. Lin, C.-L. Lin, C.-C. Wu, T.-C. Chao, K.-T. Wong, *Org. Electron.* **2007**, *8*, 189.
[14] D. Yokoyama, A. Sakaguchi, M. Suzuki, C. Adachi, *Appl. Phys. Lett.* **2009**, *95*, 243303.
[15] D. Yokoyama, Y. Setoguchi, A. Sakaguchi, M. Suzuki, C. Adachi, *Adv. Funct. Mater.* **2010**, *20*, 386.
[16] D. Tanaka, H. Sasabe, Y.-J. Li, S.-J. Su, T. Takeda, J. Kido, *Jpn. J. Appl. Phys.* **2007**, *46*, L10.
[17] H. Sasabe, T. Chiba, S.-J. Su, Y.-J. Pu, K. Nakayama, J. Kido, *Chem. Commun.* **2008**, 5821.
[18] J. A. Woollam, B. Johs, C. M. Herzinger, J. Hilfiker, R. Synowicki, C. L. Bungay, *Proc. SPIE* **1999**, *CR72*, 3.
[19] I. M. Ward, in *Structure and Properties of Oriented Polymers*, Applied Science Publishers, London, UK **1975**.
[20] B. Servet, S. Ries, M. Trotel, P. Alnot, G. Horowitz, F. Garnier, *Adv. Mater.* **1993**, *5*, 461.
[21] Z.-A. Jian, Y.-Z. Luo, J.-M. Chung, S.-J. Tang, M.-C. Kuo, J.-L. Shen, K.-C. Chiu, C.-S. Yang, W.-C. Chou, C.-F. Dai, J.-M. Yeh, *J. Appl. Phys.* **2007**, *101*, 123708.
[22] U. Ziener, J.-M. Lehn, A. Mourran, M. Möller, *Chem. Eur. J.* **2002**, *8*, 951.
[23] C. Meier, U. Ziener, K. Landfester, P. Weihrich, *J. Phys. Chem. B* **2005**, *109*, 21015.
[24] U. Ziener, *J. Phys. Chem. B* **2008**, *112*, 14698.
[25] C. Meier, K. Landfester, U. Ziener, *J. Phys. Chem. C* **2009**, *113*, 1507.
[26] C. Meier, M. Roos, D. Künzel, A. Breitruck, H. E. Hoster, K. Landfester, A. Gross, R. J. Behm, U. Ziener, *J. Phys. Chem. C* **2010**, *114*, 1268.
[27] P. Hobza, Z. Havlas, *Chem. Rev.* **2000**, *100*, 4253.
[28] K. Hermansson, *J. Phys. Chem. A* **2002**, *106*, 4695.
[29] X. Li, L. Liu, H. B. Schlegel, *J. Am. Chem. Soc.* **2002**, *124*, 9639.
[30] S. Wojtulewski, S. J. Grabowski, *Chem. Phys.* **2005**, *309*, 183.
[31] A. V. Afonin, A. V. Vashchenko, *J. Mol. Struct.: THEOCHEM* **2010**, *940*, 56.
[32] J. L. Alonso, S. Antolínez, S. Blanco, A. Lesarri, J. C. López, W. Caminati, *J. Am. Chem. Soc.* **2004**, *126*, 3244.
[33] H. Yoshida, A. Ehara, H. Matsuura, *Chem. Phys. Lett.* **2000**, *325*, 477.
[34] H. Sasabe, D. Tanaka, D. Yokoyama, T. Chiba, Y.-J. Pu, K. Nakayama, M. Yokoyama, J. Kido, *Adv. Funct. Mater.* **2011**, *21*, 336.
[35] H. Bässler, *Phys. Status Solidi B* **1993**, *175*, 15.
[36] P. M. Borsenberger, J. J. Fitzgerald, *J. Phys. Chem.* **1993**, *97*, 4815.
[37] H. Ishii, K. Sugiyama, E. Ito, K. Seki, *Adv. Mater.* **1999**, *11*, 605.
[38] S. Nowy, J. Frischeisen, W. Brütting, *Proc. SPIE* **2009**, *7415*, 74151C.